CERN-LHCb-PUB-2009-012

LPHE-2009-03

Alignment of the Inner Tracker Stations Using First Data.

L. Nicolas, M. Needham
Laboratoire de Physique des Hautes Énergies,
École Polytechnique Fédérale de Lausanne

November 6, 2009

Abstract

Data taken during LHC synchronisation tests in August–September 2008 has been used to align the Inner Tracker ladders with a precision of 20 μm. To validate the results, simulation studies with a high multiplicity particle gun have been performed. In addition, alignment studies with data taken with a cosmic trigger are discussed.

1 Introduction

The LHCb Inner Tracker [1] consists of twelve boxes placed around the beam pipe in four stacks of three boxes, as shown in Fig. 1 for a single station. Each of these boxes contains four layers of seven silicon-strip modules called ladders. There are two X layers (X1 and X2) with vertical strips and two stereo layers (U and V) with strips tilted by $\pm 5^\circ$ to allow 3D track reconstruction.

After the construction of the detector, a survey of the Inner Tracker was performed [2]. In the survey, the position of the X ladders and X layers was determined with an accuracy of $50\,\mu$m. A survey of the stereo layers was not possible as they were visually obscured by the X layers. Since each stereo layer is mounted on the same cooling rod as an X layer, it was assumed that the corrections found for the position of the X layers were valid for the corresponding stereo layer. After installation of the detector in the experimental area, the position of the boxes was surveyed with a precision of $500\,\mu$m. This was carried out whilst part of the detector was in the open position and does not include possible systematic shifts during the opening and closing procedures. Taking these into account, an overall precision of 1 – 2 mm is quoted on the box positions [2].

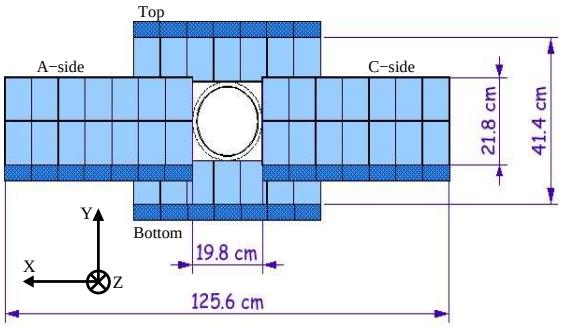

Figure 1: Layout of an Inner Tracker station.

In [3], a first alignment of the Inner Tracker boxes and layers in the most sensitive coordinate (x) is discussed. Using a technique based on histogramming of residuals these studies validated the correctness of the survey and provided first alignment constants.

In the Summer of 2008, synchronisation tests were carried out by the LHC machine. During these tests, shots of $2 - 5 \times 10^9$ protons with an energy

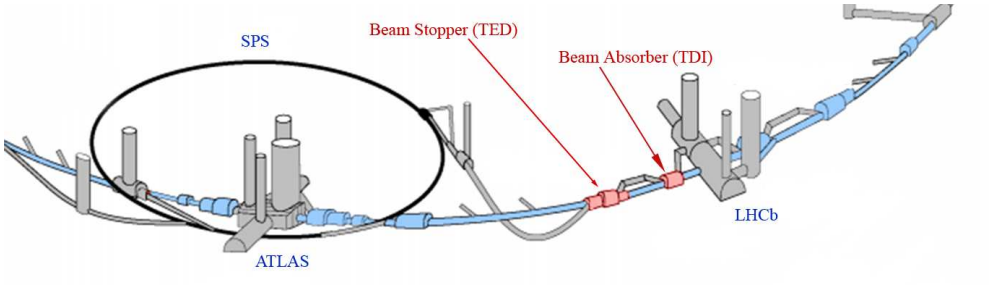

Figure 2: Layout of the LHC and SPS rings showing the LHCb experimental area and the TED beam stopper 350 m downstream.

of 450 GeV were extracted from the SPS and dumped onto a beam stopper, the 'TED', situated 350 m downstream of LHCb (as shown in Fig. 2). This created a spray of particles which gave a clear signal in the detector. Though the track density is high – more than twenty times that expected in normal running, the tracks have high momentum and the magnetic field is off. This simplifies the pattern recognition and allows reliable track reconstruction to be performed.

A full Monte Carlo simulation of the TED data was performed. In this FLUKA-based simulation, 10^9 protons were dumped onto the TED and the products transported through the various elements of the beam line to the entrance of the LHCb cavern. From this point the standard LHCb simulation chain (Boole and Gauss) was used for processing. First results from this simulation indicate that the majority of particles that give hits in the IT are 10 GeV muons (as shown in Fig. 3) decaying from pions produced in the TED.

Alignment with a data sample of events collected with a cosmic trigger is also studied. The low statistics in this case does not allow a precision alignment of the Inner Tracker, but demonstrates that the method can be used with this type of tracks.

2 Alignment with TED Run Data

The following sections present studies of Inner Tracker alignment performed with the TED data. First, the procedure is described. Next, some features of the TED data are discussed using Monte Carlo simulation, followed by a

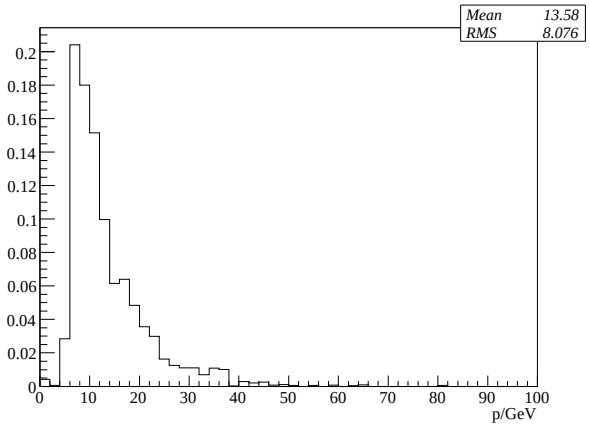

Figure 3: Momentum distribution of the muons produced in the TED. This plot shows the result of the full Monte Carlo simulation discussed in the text. The histogram is normalised such that the area is unity.

description on the track and event selection. Finally, the results of the alignment are discussed and validated by studying the evolution of the unbiased residuals [1] distributions during the alignment procedure.

Throughout the result section, the following convention is used: the degrees of freedom are called Tx, Ty and Tz (translation of the detector elements along the horizontal measurement direction, the vertical direction and the beam axis, respectively) and Rx, Ry and Rz (rotations about the three axes).

2.1 Procedure

In these studies, each of the four stacks of detector boxes are individually aligned and no account is taken of the fact that $\sim 1\,\%$ of the tracks pass through the overlap region between the side and the Top/Bottom boxes. This is because the high occupancy and misaligned detector make it difficult to find such tracks.

The reconstruction software sequence is shown in Fig. 4. After collecting the IT clusters, the ITGenericTracking algorithm described in Ref. [6] is

[1] Unbiased residuals are residuals calculated by re-fitting the track without taking into account the information from the current hit.

run. Then the tracks are fitted with the standard LHCb track-fitting code [7]. Obvious ghost tracks [2] are removed by applying an evolving cut on the track χ^2 (TrackContainerCleaner). Next, an algorithm that ranks the tracks according to their number of hits and χ^2 is run to remove ghosts and clones and to select the optimal subset of tracks (TrackCompetition). After this sequence is run, the track quality and parameters can be monitored using the standard LHCb monitoring tools. In parallel, the alignment algorithm is run on the selected set of tracks. Finally, the algorithm produces a set of new alignment constants, which are used in the next iteration of the procedure.

As discussed in Ref. [4], a multi-step approach to the alignment is needed for two reasons. First, large overall misalignments in the measurement direction (more than $\sim 100\,\mu$m) cannot be recovered at the ladder level. The second reason is that layers and ladders cannot be aligned in the vertical (y) direction as they are only weakly sensitive to this parameter. Only global y alignment at the box granularity can be obtained. Furthermore, the available statistics and the small angle of the tracks in the TED run mean that the data is not sensitive to other degrees of freedom, such as movements along the z axis (Tz).

Therefore, the following approach is chosen:

1. Alignment of boxes in Tx, Ty and Rz;
2. Alignment of layers in Tx and Rz;
3. Alignment of ladders in Tx.

A priori, other choices are possible: for example, alignment at the box level, ignoring possible shifts in y or alignment of ladders after boxes, without alignment of the layers. Studies of several of these possibilities were made and found to give identical results in terms of number of reconstructed tracks and unbiased residuals. This shows that the data does not allow to fully determine the best procedure. However, as discussed in Section 2.5, it is possible to justify the choice of Rz as an alignment parameter. The above scenario is chosen because it deals with more degrees of freedom and hence seems more complete.

To constrain the global movements, the following objects are fixed during the procedure:

[2] Ghost tracks are reconstructed with hits from more than one particle [8].

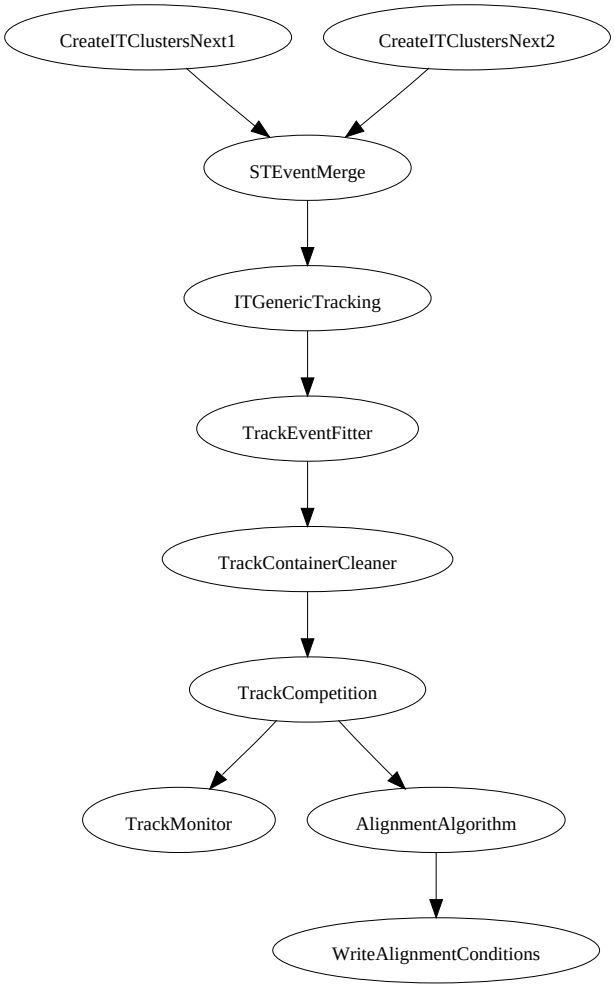

Figure 4: Flow diagram of the software procedure used for the tracking-station alignment with TED data.

Table 1: Summary of the misalignments applied in the realistic misalignment scenarios used with the Monte Carlo sample of TED-like simulated events. The amplitude is the width of the flat distribution used to generate the misalignments.

Elements	DoF	Scenario 1	Scenario 2
X layers	Tx [mm]	0.3	0.03
Stereo layers	Tx [mm]	0.3	0.3
All layers	Rz [mrad]	2.5	2.5
Ladders	Tx [mm]	0.1	0.1

1. For the box alignment, all boxes in Stations 1 and 3 are fixed.
2. For the layer alignment, the two first layers in Station 1 (X1 and U) and the two last layers in Station 3 (V and X2) are fixed.
3. For the ladder alignment, all the ladders from the two first layers in Station 1 (X1 and U) and from the two last layers in Station 3 (V and X2) are fixed.

This leaves a total of three degrees of freedom (Tx, Ty and Rz) per box type for the box alignment, 16 degrees of freedom (Tx and Rz for each of the eight free layers) per box type for the layer alignment and 56 degrees of freedom (Tx for each of the eight layers $\times$ seven ladders) per box type for the ladder alignment.

2.2 Results from Monte Carlo Events Simulating TED Data

This section presents the results obtained with a Monte Carlo simulation of TED-like events (not the complete FLUKA-based simulation). In these studies, a high multiplicity muon gun is used to mimic the TED environment. The track angles and origin are similar to those expected for particles produced in the TED. Particle energies of 5, 10, 20, 40 and 80 GeV are simulated in events with densities in the Inner Tracker between 0.01 and 0.08 particles per cm^2.

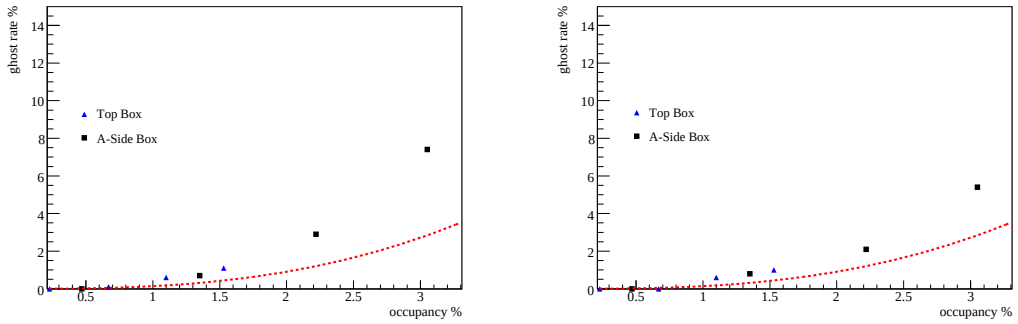

(a) misalignment scenario 1 (b) misalignment scenario 2

Figure 5: Ghost rate in the Monte Carlo simulated TED-like data sample as a function of the IT occupancy for the two misalignment scenarios given in Table 1. The points show the ghost rate with a misaligned database, whereas the dotted curve is obtained with an ideal detector.

The performance of the pattern recognition is studied using these data with two misalignment scenarios, which are summarised in Table 1. Only the misalignment for the x translation is different for the two scenarios. A flat distribution is used to generate random misalignment values. The amplitude of the Tx distribution is of $300\,\mu$m for the X layers in scenario 1 and for the stereo layers in both scenarios and $30\,\mu$m for the X layers in scenario 2. The layers are also rotated about the z axis by up to 2.5 mrad. Finally, all ladders are misaligned in Tx with an amplitude of up to $100\,\mu$m. The second scenario considered has misalignment scales close to those thought to remain after the pre-alignment studies discussed in Ref. [3]. Figures 5 and 6 show the ghost rate and efficiency as a function of the detector occupancy. It can be seen that compared to the ideal detector, the ghost rate is significantly increased at high occupancies. However, the efficiency is reduced by only a few percent.

The ghost rate and track reconstruction efficiency in TED data can be extrapolated from the plots in Figs. 5 and 6, knowing that the detector occupancy is $\sim 4\,\%$ for the A-/C-side boxes and $\sim 2\,\%$ for the Top and Bottom boxes. The extrapolated numbers for the two misalignment scenarios are given in Table 2 for the A-side and the Top boxes. The tight selection criteria presented in Section 2.3 (with a cut at $\chi^2/\text{dof} < 20$) reduce the ghost rate to $1.4\,\%$ for the A-side box and a negligible value for the Top box, where the occupancy is significantly lower. The reconstruction efficiencies are somewhat low, but the emphasis is on having a high purity track sample.

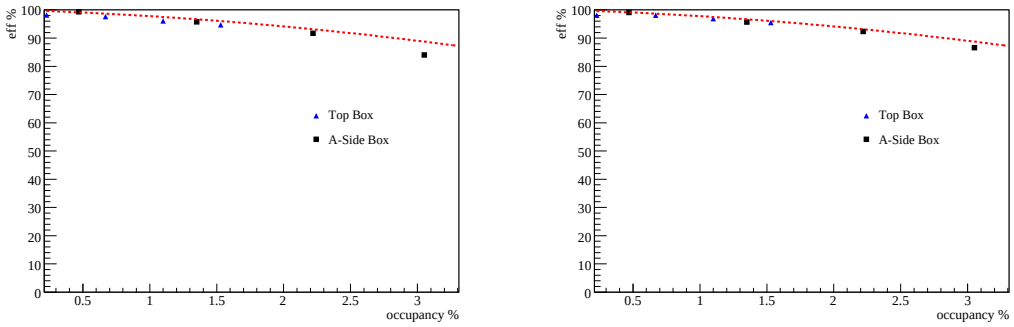

(a) misalignment scenario 1 (b) misalignment scenario 2

Figure 6: Track-reconstruction efficiency in the Monte Carlo simulated TED-like data sample as a function of the IT occupancy for the two misalignment scenarios given in Table 1. The points show the ghost rate with a misaligned database, whereas the dotted curve is obtained with an ideal detector.

Table 2: Ghost rates and track-reconstruction efficiencies extrapolated from the Monte Carlo simulated TED-like data sample to the detector occupancies in the real TED data, as a function of the misalignment scenario.

	Ghost rate		Efficiency	
Misalignment scenario	A-side box	Top box	A-side box	Top box
None (ideal detector)	6 %	1 %	82 %	94 %
Scenario 1	18 %	2 %	73 %	93 %
Scenario 2 (“realistic”)	12 %	1 %	78 %	95 %
Tight cuts [6]	1 %	0 %	68 %	93 %

Table 3: Strategy for the evolving cut on the track χ^2/dof for each step of the alignment procedure.

	Iteration			
Alignment step	1	2	3	> 4
Box alignment	250	100	50	30
Layer alignment	100	80	50	20
Ladder alignment	100	80	50	20

In Ref. [4], an evolving cut on the track χ^2 is presented and shown to improve the results of the alignment. A similar strategy is used here. The plots in Fig. 7 show the distribution of the track χ^2/dof after selection for tracks going through the Top box running with the realistic misalignment scenario 2 given in Table 1 and the ideal geometry, respectively. The cut in the first iteration is chosen to be loose: $\chi^2/\text{dof} < 250$ for the box alignment (first step in the procedure) and $\chi^2/\text{dof} < 100$ for the layer and ladder alignment, when the large misalignments are already corrected for. A reasonable cut value in the last iteration is at $\chi^2/\text{dof} < 20$. This does not bias the track sample whilst rejecting most of the ghost tracks before the track competition algorithm [3]. The sequence for the cut on the track χ^2/dof is given in Table 3.

Finally, the simulation can be used to estimate the width of the unbiased residuals distributions as a function of the track momentum. The results are shown in Fig. 8. The resolution is shown separately for X and stereo layers. This is because all twelve layers per box type contribute to the measurement in the x direction, while only the six stereo layers contribute to the measurement in the y direction, leading to the residual being a factor of $\sqrt{2}$ worse. This plot can be used in two different ways. Knowing the momentum, the expected resolution of the unbiased residuals can be derived. Comparison of this number and the resolution obtained with data before alignment allows the residual misalignment to be estimated. On the other hand, if the residual misalignment can be correctly estimated from survey measurements or another method, the resolution found for the unbiased residuals gives an estimate of the average track momentum. Assuming a track momentum of $\sim 10\,\text{GeV}/c$, as given by the first studies with the FLUKA-based simulation discussed in the introduction, a residual ladder misalignment of $\sim 85\,\mu\text{m}$ is estimated for the stereo layers and $60\,\mu\text{m}$ for the x layers.

[3] The cut is applied in the TrackContainerCleaner algorithm.

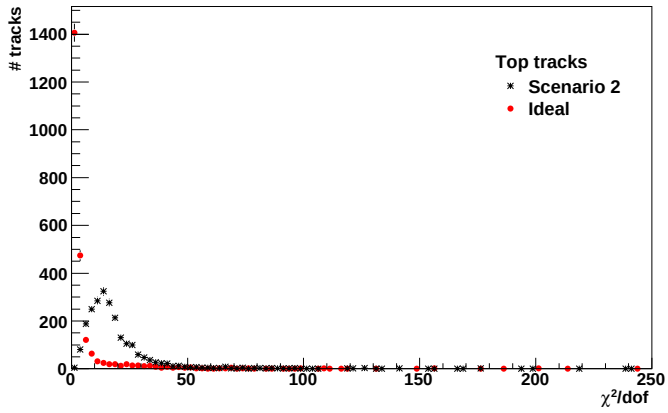

Figure 7: Distribution of track χ^2/dof after the track selection for tracks going through the Top box. Both the distributions with the misalignment scenario 2 and with the ideal geometry are shown. The data used is the Monte Carlo sample of TED-like simulated events.

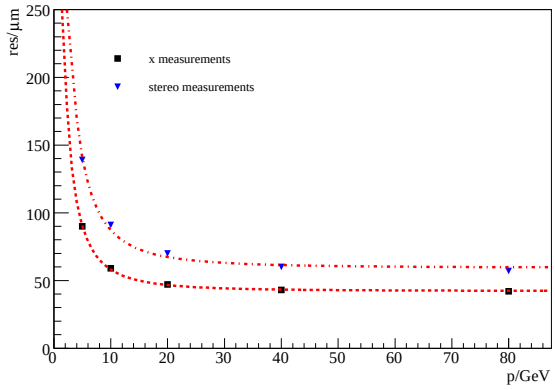

Figure 8: Resolution of the unbiased residuals in the Top Box as a function of the average track momentum for Monte Carlo simulated TED-like data. The results are shown for the X and stereo layers separately.

2.3 Track and Event Selection

The principal difficulty with the data collected during the synchronisation tests is the high occupancy [6]. Figure 9 shows a typical event from the 2009 TED run with the IT in its open position (see Section 3). The twelve IT boxes are shown with the active area in red and the particles crossing the detector in blue. The larger red areas correspond to the A- and C-side boxes. There are twenty times more hits per event than expected in normal LHCb running conditions. For the side boxes where the strips are longest, the track multiplicity is larger than for the Top and Bottom boxes. This leads to a sizable ghost rate, which degrades the quality of the alignment. To reduce the ghost rate, relatively low occupancy events are used. For the box and layer alignment, the statistics are high enough to align every element with at least 50 hits, even when rejecting the events where the occupancy is too high (more than 4500 clusters in the IT, corresponding to a 3.5 % occupancy). However, for the ladder alignment, where the number of hits per element is much smaller, this requirement is released to 5000 clusters per event in order to align every element with at least 25 hits [4]. With this requirement, the statistical precision is better than $\frac{57\,\mu\text{m}}{\sqrt{25}} \approx 11.4\,\mu\text{m}$ for the ladder alignment. However, releasing the requirement on the maximum number of clusters increases the ghost rate of about 0.4 %, which in turn adds a small systematic error on the resolution.

A second way to reduce the ghost rate is to use tight search windows in the pattern recognition. However, since the detector is misaligned, care is needed that search windows are not set too small. Based on the results presented in Refs. [3, 6], windows of 0.8 mm in the x direction and 10 mm in the y direction are chosen for the first step of the procedure described in Section 2.1. Assuming 100 μm misalignments remain for the x-measuring ladders and 200 μm for the stereo ladders, these cuts correspond to 4 or 5 σ windows.

Finally, the evolving cut on the track χ^2/dof described in Section 2.2 is used. The value of the cut at each iteration is given in Table 3. Figure 10 shows the same distributions as in Fig. 7 with the real data. The plot on the left shows the distribution before alignment and on the right after the complete alignment procedure described in Section 2.1. The distribution obtained with the misalignment scenario 2 in Fig. 7 corresponds to the distribution before alignment in Fig. 10, whereas the distribution with the ideal geometry in

[4] At this stage, smaller search windows are used, reducing the ghost rate and allowing the requirement on the maximum number of hits to be relaxed.

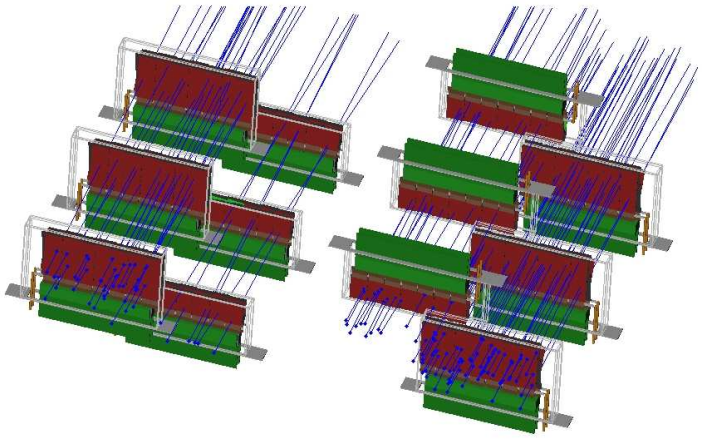

Figure 9: Panoramix event display of a typical event from the 2009 TED run where the IT is opened (see Section 3). The particles crossing the Inner Tracker are shown in blue. The red areas correspond to the IT active area. The larger boxes are the side boxes.

Fig. 7 should match the distribution after alignment in Fig. 10 in case of a perfect alignment. As visible in the latter, the distribution is a broader than in the case of an ideal alignment. This effect can be related to the ghost tracks in the sample used.

As discussed in Ref. [6], the pattern recognition performance can be improved once the detector is aligned by reducing the size of the search windows in the pattern recognition. After the box alignment in y, the y search-window is tightened from 10 mm to 7 mm for the subsequent steps. Similarly, the window in x is tightened from 0.8 mm to 0.5 mm after the box alignment.

2.4 First Alignment of the Inner Tracker in the x Measurement Direction

The following two sections present the results of a first alignment of the Inner Tracker boxes and layers for the most obvious degree of freedom, the translation along the horizontal x axis.

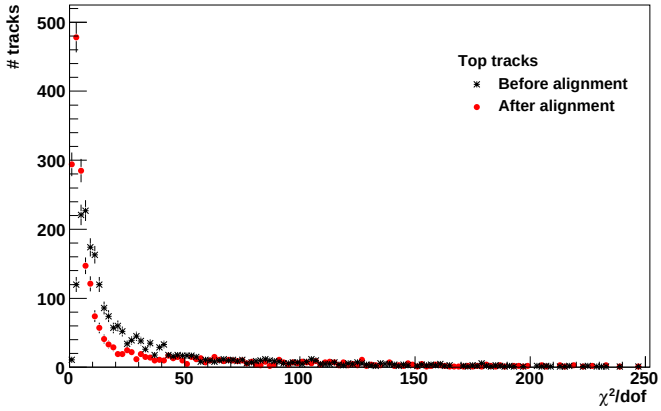

Figure 10: Distribution of track χ^2/dof after the track selection for tracks going through the Top box. Both the distributions before and after the alignment procedure are shown. Both distributions are obtained with the loose pattern recognition search-windows.

2.4.1 Alignment of Boxes in x

The software alignment of the IT is performed for the boxes in Station 2 only in the measurement direction (Tx). The geometry used as a starting point is the survey geometry described in Ref. [2]. The results of the alignment for the A-/C-side boxes are reported in Fig. 11 (a), whereas the results for the Top/Bottom-box alignment are reported in Fig. 12. The first observation is that the two alignment jobs converge, although it takes five iterations to the procedure to find the optimal position of the boxes. This relatively slow convergence is due to the large misalignments compared to the size of the search windows in the pattern recognition. Except for the Bottom box, which moves by 100 μm, the three other boxes move by 700–800 μm.

In order to check the validity of these results, the alignment procedure is then run starting from another database, the output of the pre-alignment discussed in Ref. [3]. The results of the alignment of the A- and C-side boxes can be seen in Fig. 11 (b), whereas the results of the Top/Bottom-box alignment is reported in Fig. 12 (b).

From these two sets of plots, it can be seen that the alignment procedure converges within 60 μm to the same position. That is to say, whatever the assumed initial position of the detector, the alignment moves it to the same

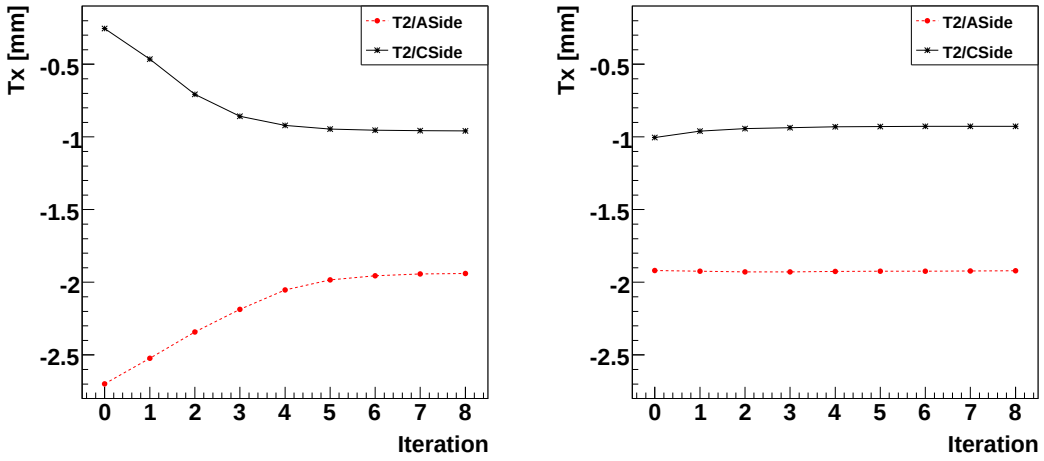

(a) survey geometry (b) best pre-aligned geometry

Figure 11: Evolution of the Tx alignment constant during A- and C-side-box alignment, (a) starting from the surveyed geometry and (b) starting from the geometry given by the method described in Ref. [3].

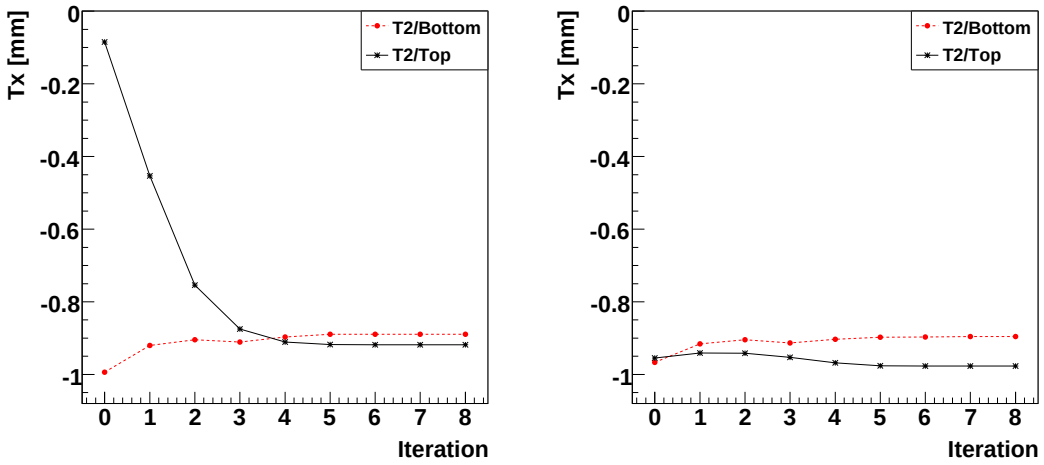

(a) survey geometry (b) best pre-aligned geometry

Figure 12: Evolution of the Tx alignment constant during Top- and Bottom-box alignment. (a) shows the alignment starting from the surveyed geometry and (b) starting from the geometry given by the method described in Ref. [3].

point (last points from plots (a) and (b) in Figs. 11 and 12). It can be seen that the alignment described in Ref. [3] is consistent within 100 μm with the alignment parameters determined with the software alignment, if a movement in x only is assumed. However, this alignment scenario is simplistic and doesn't take other degrees of freedom into account. Section 2.5 discusses the alignment of the detector elements for the rotation around the z axis and shows that it needs to be accounted for. Furthermore, the translation along the vertical axis is also important, as shown in Section 2.6.1. However, this first simple study shows that, although it is not necessary in the alignment procedure, the results from Ref. [3] are a better starting point than the survey measurements.

2.4.2 Alignment of Layers in x

Another consistency check is possible between these results and the geometry database based on the results given in Ref. [3]. In the first alignment studies performed using the software method (which are not reported in this document), movements of several hundreds of microns were seen for some stereo layers, but not for the corresponding X layer. As those layers are mounted on the same cooling rod, they should move together. It was found that these apparent movements were due to wrong pre-alignment values for the pairs of X and stereo layers. After correcting these mistakes, the expected correlation between the movements of the X and stereo layers is seen. The precision of this assumption can be tested using the data itself. Figure 13 shows the correlation between the total corrections for the translation in x applied to an X layer and to its corresponding stereo layer [5]. The distribution of the difference between the two corresponding corrections has an RMS of $\sim 130\,\mu$m. This should be compared to the mean and RMS of the layer survey corrections in x of 400 and 285 μm, respectively.

2.5 Justification of the Alignment in Rz

The alignment of the Inner Tracker detector elements for translations in the x direction is natural since this is the most sensitive degree of freedom. Aligning the boxes for the translations in y is also easy to justify through the combination of X and stereo layers. Apart from these two degrees of freedom,

[5] This information is available for both the X and the stereo layers because 3D tracks are used to align the detector.

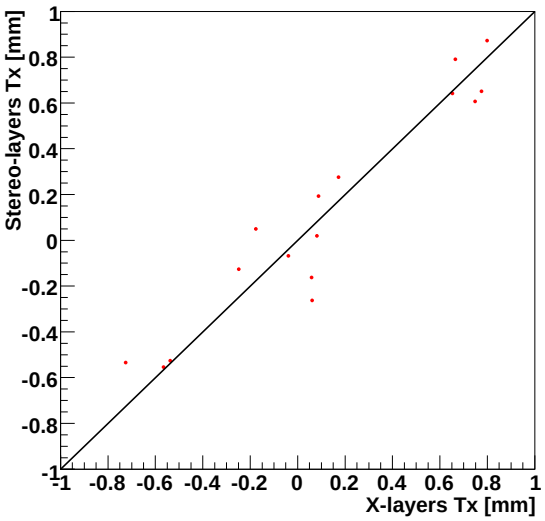

Figure 13: Correlation between the total Tx corrections applied to the stereo layers and to their corresponding X layers. The values plotted are after alignment of the layers in Tx. Only the layers being aligned are shown.

the detector is also sensitive to the rotation Rz around the z axis, which is coupled to the measurement in the x and y directions, since a rotation of a box around its z axis can be transformed into a gradient in the y direction of translations along the x axis. That is to say that if the box is sliced along the y axis and only the alignment in Tx is considered, each slice should have different corrections.

In order to further justify the choice of the Rz parameter in the alignment procedure, the following analysis is performed. Four 3 cm slices are defined in the Top and Bottom boxes, with the centres along the y axis being at ± 10.5 cm, ± 13.5 cm, ± 16.5 cm and ± 19.5 cm from the beam axis. As the illumination of the boxes is uniform, the same number of hits is seen in each slice. The alignment procedure is then run, aligning these two boxes for Tx only. The two plots in Fig. 14 show that each slice needs a different correction, with a linear shape. This is expected in case the boxes are rotated around their z axis. The same method is used on the A- and C-side boxes and gives similar results. This justifies the alignment for Rz as well as Tx for the boxes and layers, as discussed in Sections 2.6.1 and 2.6.2. The other degrees of freedom (translation along the beam axis and rotations around the x and y axes) are harder to align for because the Inner Tracker geometry implies a smaller sensitivity to these.

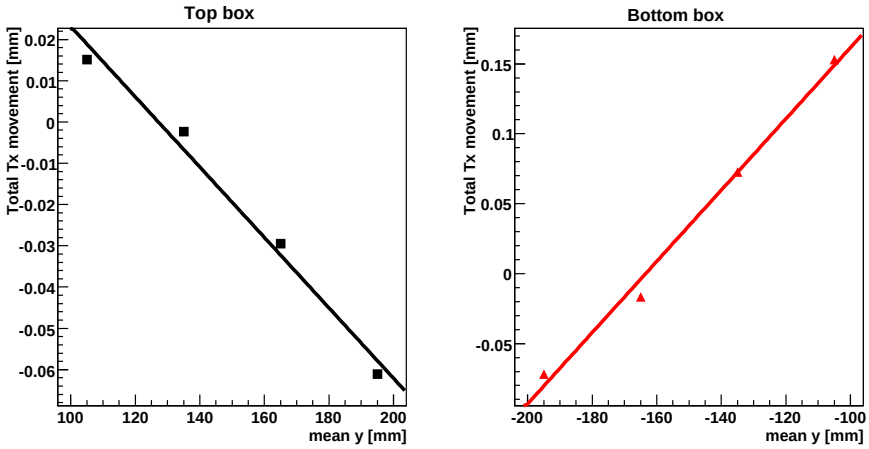

Figure 14: Corrections needed in the x direction for slices in y of the Top and Bottom boxes in case only Tx is aligned for in the procedure.

2.6 Alignment Results

2.6.1 Box Alignment

The first step of the full alignment procedure is to align the boxes in Station 2, with the constraint that the boxes in Station 1 and 3 are fixed. From Ref. [3], the box alignment in x is known to be precise within 100 μm. However, this doesn't take into account rotations, especially around the beam axis, which are correlated to the movements in the x measurement-direction, as discussed in the previous section. A proper software alignment of the Inner Tracker boxes is hence performed using the method discussed in Refs. [4] and [5], starting from the output of the alignment described in Ref. [3]. The procedure used is described in Section 2.1. Figures 15 (a) and (b) show the evolution of the alignment parameters of the A- and C-side boxes, respectively the Top and Bottom boxes.

The side boxes move in x by respectively 7 and 45 μm, which is inside the precision of 100 μm quoted in Ref. [3]. On the other hand, the Top and Bottom boxes move by 125 and 423 μm, respectively. Both these movements are correlated to large rotations around the beam axis. These rotations could explain the discrepancy between the results quoted in Ref. [3] and the survey measurements given in Ref. [2].

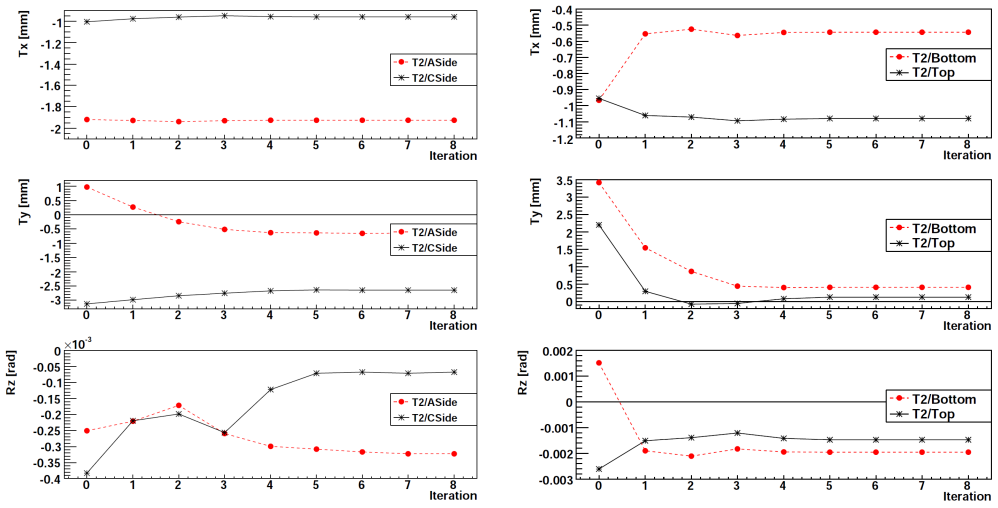

(a) A- and C-side box alignment (b) Top and Bottom box alignment

Figure 15: Evolution of the Tx, Ty and Rz alignment parameters during the box alignment for (a) A- and C-side boxes and (b) Top and Bottom boxes.

The movement in the y direction of the Top and Bottom boxes is 2.1 and 3.0 mm, respectively. The A- and C-side boxes move by 1.6 and 0.5 mm. As discussed in Section 1 the survey was carried out with part of the detector in the open position. One explanation for these large movements is that the detector position changed during the closing of the other Inner Tracker and Outer Tracker half-stations.

The first method to check whether the alignment has converged properly is to look at the normalised total sum of track χ^2/dof. Figures 16 (a) and (b) show that the alignment procedure has converged in four iterations both for the side boxes and for the Top and Bottom boxes. The steps in these plots are due both to the convergence of the alignment procedure (which minimises the total sum of track χ^2), and to the evolving cut on the track χ^2/dof described in Section 2.3. The value of the track χ^2/dof after alignment of 10 and 12 for the A-/C-side and Top/Bottom boxes respectively seems surprising at first. However, this large value can be explained. First, due to the large occupancy, two close-by clusters can be merged in one 3–4 strip cluster. This degrades the track χ^2. Next, after these studies have been performed, it was realised that the track fit assumed the track had five degrees of freedom (x, y, tx, ty, q/p). Correcting this to four for the case of the magnet-off running improves the χ^2/dof distribution by $\sim 10\,\%$. Finally, the multiple scattering is not taken into account in the track fit, which adds a third effect.

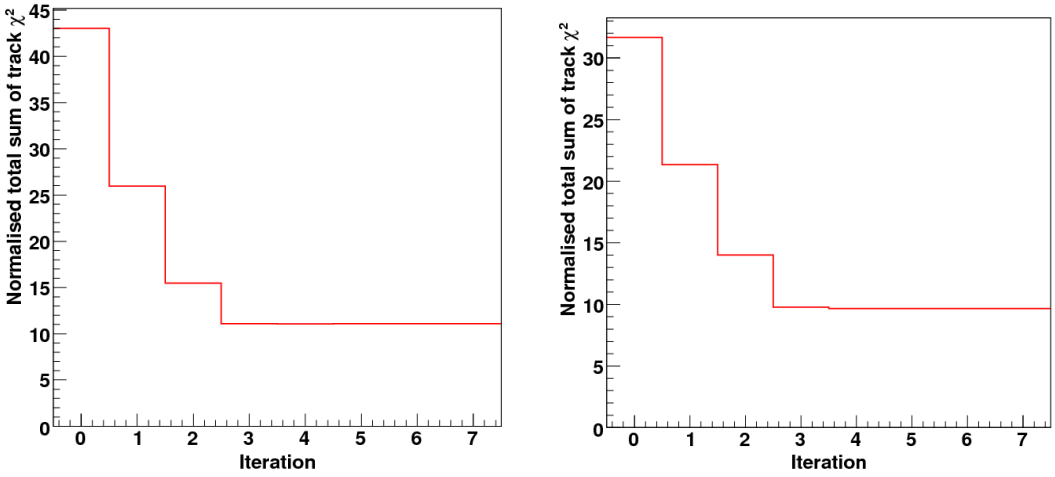

(a) A- and C-side box alignment (b) Top and Bottom box alignment

Figure 16: Convergence of the normalised total sum of track χ^2/dof during box alignment in Tx, Ty and Rz for (a) A- and C-side boxes and (b) Top and Bottom boxes. The histogram shows the value of the track χ^2/dof averaged on the track sample.

2.6.2 Layer Alignment

The results of the alignment of the layers in the A- and C-side boxes and in the Top and Bottom boxes are shown in Figs. 17 (a) and (b), respectively. The studies described in Ref. [3] showed that the X layers were aligned with a precision of $\sim 30\,\mu$m. The top two plots show that apart from two layers in the Top boxes (Station 3 / Top box / Layer X1 and Layer U) and two in the C-side boxes (Station 1 / C-side box / Layer V and Station 3 / C-side box / Layer U) that move by up to $190\,\mu$m, all the other layers move inside a $60\,\mu$m window around their initial position (corresponding to the result of the first alignment described in Ref. [3] plus the corrections to the boxes in Station 2 applied in the first step of the alignment procedure). The large movements of the four layers found above is justified by the fact that the constraints in the box alignment and in the layer alignment are not the same. In the first step, all layers in Stations 1 and 3 are fixed, while in the second step, the first two layers in Station 1 and the last two layers in Station 3 are fixed. This difference causes some global adjustments in the layer alignment step, to which the outer layers are more sensitive (especially since they were not aligned with their corresponding boxes in the first step). In addition, the stereo layers were not aligned in the procedure described in

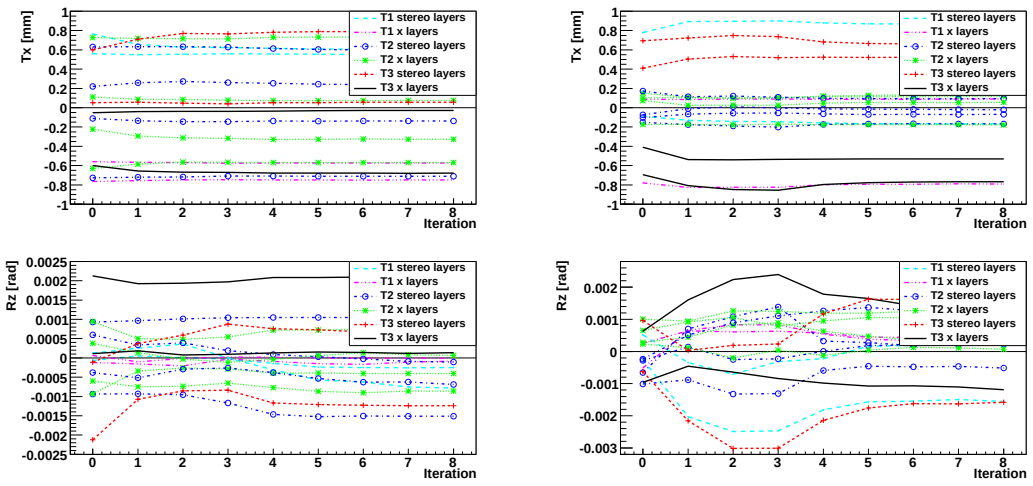

(a) A- and C-side layer alignment (b) Top and Bottom layer alignment

Figure 17: Evolution of the Tx and Rz alignment parameters during layer alignment for (a) A- and C-side layers and (b) Top and Bottom layers.

Ref. [3] and the Rz rotation not taken into account. These effects explain the discrepancy between the average movements found with the two different methods discussed.

Figures 18 shows that the alignment has converged in four iterations. As for the boxes, this slow convergence is partly due to the evolving cut on the track χ^2. Small oscillations in iterations five to seven are visible for the Top/Bottom boxes. They are due to tracks being picked up and dropped between two subsequent iterations. A slight movement of the detector after one alignment iteration changes the output of the track finding. Since the track sample is different, the result of the alignment algorithm differs, moving again the detector.

2.6.3 Ladder Alignment

The next step is to align the ladders. Care needs to be taken to check that movements of all the elements are mechanically allowed. As discussed before, two layers of the Inner Tracker are mounted along an aluminium cooling rod. This pipe enters through a side wall of the box, crosses the box and is bent before the opposite wall such that it runs back across the box and exits it on the same side it entered [10]. A picture of this can be seen in Fig. 19. Care

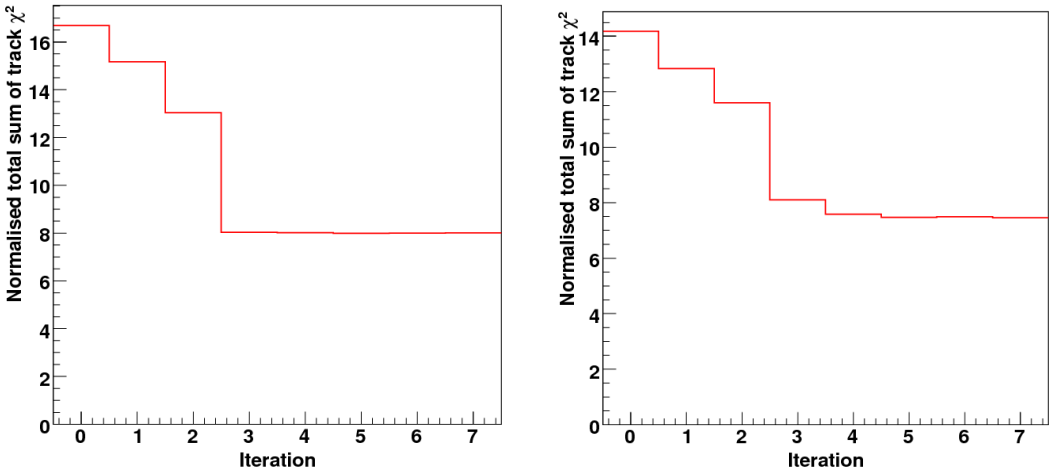

(a) A- and C-side layer alignment (b) Top and Bottom layer alignment

Figure 18: Convergence of the normalised total sum of track χ^2/dof during layer alignment in Tx and Rz for (a) A- and C-side layers and (b) Top and Bottom layers.

was taken to mount the ladders on a perfect plane along the rods. However, it was noticed during the survey that some ladders were misaligned due to the bending. Ref. [2] quotes that the position of some ladders near the cooling-rod bending have been corrected by up to 300 μm. This is taken as an estimate of the maximum allowed movement for the ladders relative to the surveyed position.

Showing the evolution of the alignment parameters for all ladders is not meaningful because of the large number of elements. A better way to show the result is to histogram the total movement in the Tx direction for all the ladders in the A-/C-side boxes and in the Top/Bottom boxes, as shown in Figs. 20 (a) and (b), respectively. Since fitting a Gaussian to these histograms is not satisfactory, the RMS of the distributions is quoted. For the A- and C-side boxes, the RMS is 123 μm, whereas for the Top and Bottom boxes, it is 202 μm. A single Gaussian fitted through the core of the distribution gives $\sigma = 98\,\mu$m for the A- and C-side and $\sigma = 88\,\mu$m for the Top and Bottom ladders. Four ladder stacks, shown in Fig. 21, seem problematic: Ladder 1 in the A-side and Top boxes and Ladder 7 in the C-side and Bottom boxes. Some ladders have moved by up to 1 mm in the Top and Bottom stacks and up to 0.5 mm in the A- and C-side stacks. This is significantly larger than the largest deviation expected from the bending of the cooling rod. Part of this

Figure 19: Photo of the IT layers fixed to the aluminium cooling rod. Both the X and stereo layers are visible, as well as the cooling-rod bending on the right of the picture.

issue could be solved by aligning the ladders for the Rz degree of freedom. This requires additional studies and will be reported in a subsequent note.

The problematic stack on the C-side is understood as one of the ladders and another nearby ladder are dead, as shown in Fig. 21, pulling the whole stack away. Dead ladders stay fixed during the alignment process. Possible corrections to a ladder in the same stack are hence biased by this artificial constraint. In addition, the problem of the cooling-rod bending can also explain the large Tx corrections.

An explanation for the Bottom stack comes from the corrections applied after the survey. Ladder 7 in the Layer X2 in Station 3 is corrected by $550\,\mu$m. However, no correction is applied to the Ladder 7 in the Layer V, as these ladders were not surveyed. As these two ladders are fixed in the alignment procedure, if there really is a mismatch, the whole stack will be pulled away. A second explanation comes from an incident that occurred during the detector installation. The Bottom box in Station 1 was damaged in an incident with another structural element. Although the box was shown to be fully operational and the box was re-surveyed after the incident, the layers and ladders were not re-surveyed. Unknown movements or rotations of some modules could account for the observed large movements in this box, which in turn induce large movements of the ladders in the Bottom boxes of the two other stations, which are connected to the problematic box by the tracks crossing the three stations.

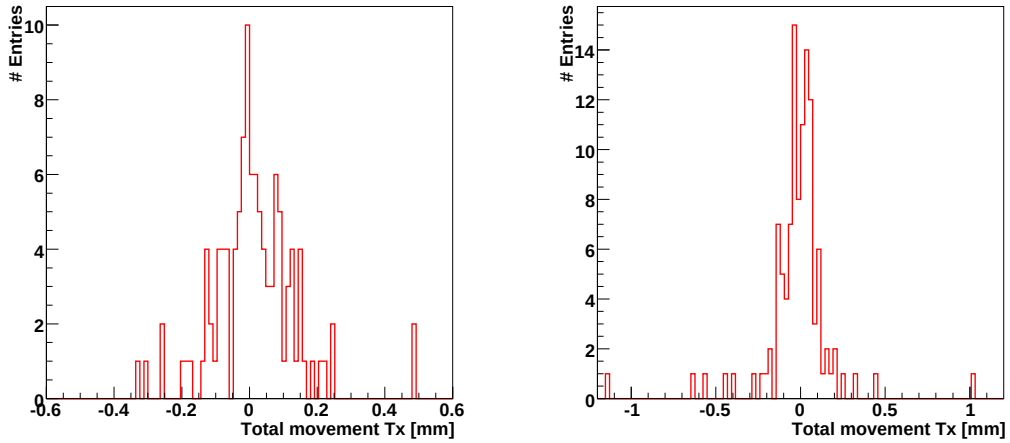

(a) A- and C-side ladder alignment (b) Top and Bottom ladder alignment

Figure 20: Distribution of the total movement in the alignment parameter Tx for all the ladders in the (a) A- and C-side boxes and (b) Top and Bottom boxes.

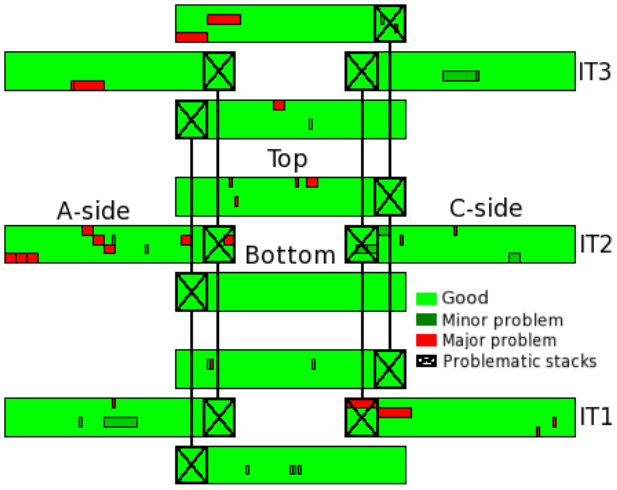

Figure 21: Schematic view of the three Inner Tracker stations showing the state of the detector at the time of the 2008 TED runs. Red zones indicate major problem, while dark green zones are minor problems. The crosses indicate the problematic ladder stacks.

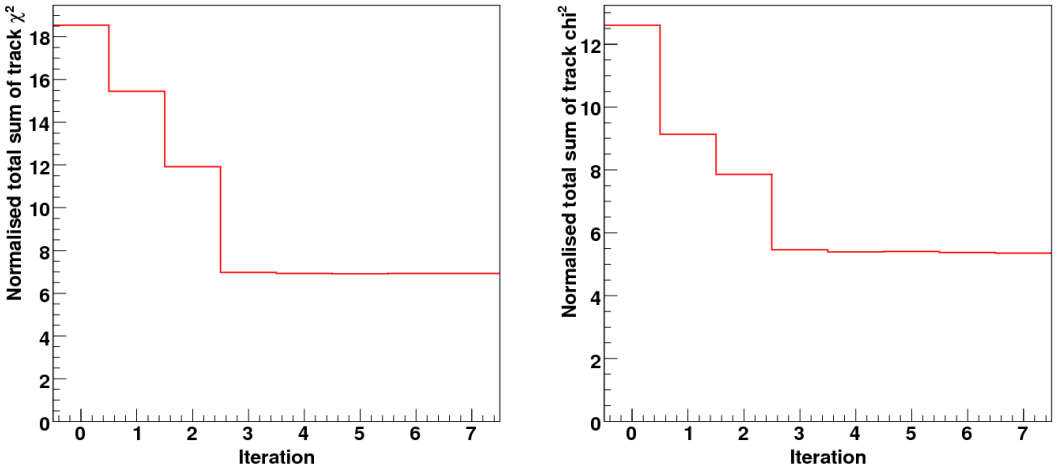

(a) A- and C-side ladder alignment (b) Top and Bottom ladder alignment

Figure 22: Convergence of the normalised total sum of track χ^2/dof during ladder alignment in Tx for (a) A- and C-side ladders and (b) Top and Bottom ladders.

The ladders in the A-side stack that are moved a lot during the alignment are either stereo ladders not corrected during the survey, but adjacent to an X ladder with large corrections, or X ladders with large corrections that are moved back towards their nominal position. In addition, this stack is located close to the bend in the cooling rod.

Finally, the problem in the Top box could come from large corrections in the survey, as in the case of the A-side box. In addition, whilst the studies described here were being performed, a problem in the cabling of one of the modules in this stack was uncovered. Each module is read out by three front-end chips. In the case of this module, the cables related to two of these were swapped. Since two thirds of the hits in this module were incorrectly decoded, this module was inefficient. Taking this swap into account does not change significantly the alignment results. The largest movement in this stack is reduced from 550 μm to 490 μm (a difference of 60 μm), but the RMS of the distribution shown in Fig. 20 does not change significantly.

Removing outliers from the distributions shown in Fig. 20, the RMS drops down to 96 μm for the A- and C-side boxes and 92 μm for the Top and Bottom boxes. Despite the problematic ladders, the alignment for all ladders again converges in three iterations on average, as seen in Fig. 22.

In order to check whether uncertainties in the survey could cause large deviations, tests were performed where the survey corrections were subtracted from the problematic ladders. Running the procedure starting from this database, the problematic stacks moved back to the same point as above. This gives confidence that the survey measurements are not responsible for the large apparent movements, and confirms the robustness of the procedure.

2.7 Validation of the Results

Two different validation methods of the alignment results are presented in the following two sub-sections. They are based on the study of the unbiased residuals and on the number of reconstructed tracks. A third method based on the study of the residuals of hits in the Tracker Turicensis with respect to Inner Tracker tracks propagated back to the TT is tried but didn't give fully satisfactory results. This is mostly due to the constraint applied on some IT layers, which doesn't allow for a relative alignment of the IT with respect to the TT. This is discussed in Appendix B.

2.7.1 Unbiased Residuals

The first method used to validate the results of the alignment is to study the unbiased residuals (defined in Section 2) of the hits on the selected tracks before and after alignment. The alignment of the Inner Tracker detector elements has two effects. First, any bias on the mean of the distribution will be corrected for (alignment of global movements). Second, the resolution will improve (relative alignment of different detector elements). For these studies, an independent data sample to that used in the alignment procedure is used.

The residual distributions of the tracks selected for the alignment procedure are obtained by running a monitoring algorithm using the misaligned geometry (output of the procedure described in Ref. [3]) and the output geometry of the full alignment procedure. The distributions are separated ladder by ladder and fitted with a single Gaussian. The bias (mean) of the fitted Gaussian curve is then used to draw the plots shown in Fig. 23. The ladders in stereo and X layers are separated as it is expected that X layers have a resolution 1.4 times better (as discussed in Section 2.2). The same distributions, but separated by layer can be found in Appendix A.

Comparing the distributions of the bias before and after alignment shows a

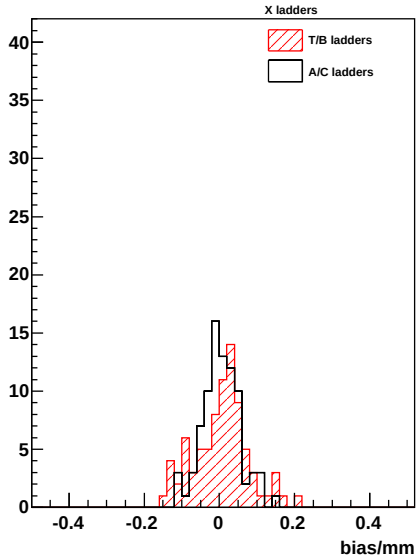

(a) X ladders before alignment

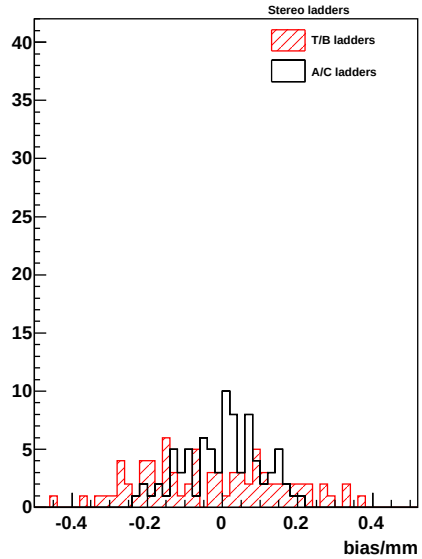

(b) stereo ladders before alignment

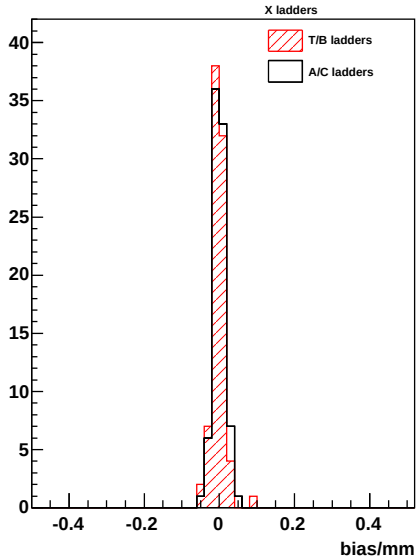

(c) X ladders after alignment

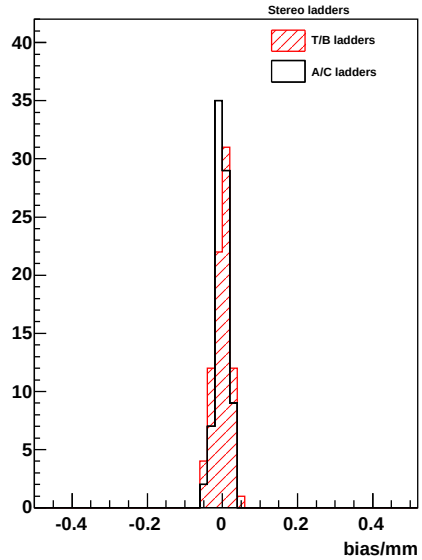

(d) stereo ladders after alignment

Figure 23: Bias of the distribution of unbiased residuals for individual ladders: (a) X ladders before alignment, (b) stereo ladders before alignment, (c) X ladders after alignment and (d) stereo ladders after alignment.

clear improvement of the unbiased residuals for all ladders. The precision of the alignment is given by the RMS of the distributions shown in Fig. 23. This precision improves from 73 and 51 μm to 19 and 17 μm for the X ladders in the Top/Bottom boxes and A-/C-side boxes, respectively. For the stereo layers, the RMS improve from 185 and 102 μm to 22 and 18 μm for the Top/Bottom and A-/C-side boxes, respectively. The overall precision of the ladder alignment is hence on average 19 μm on Tx.

The same method as discussed above is repeated, with Gaussian distributions fitted to the distributions of unbiased residuals in each of the layers. Figure 24 shows the distribution of the widths of these Gaussian fits [6]. The mean of this distribution is an indication of the spatial resolution of the detector. For the X layers, the resolution improves from 105 and 106 μm before alignment to 87 and 95 μm after alignment for the Top/Bottom boxes and the A-/C-side boxes, respectively. The evolution is from 169 and 180 μm before alignment to 126 and 148 μm for the stereo layers of the Top/Bottom and A-/C-side boxes, respectively.

The unbiased residuals therefore confirm that the alignment procedure is indeed doing the right job. The distribution of the bias of the unbiased residuals shows that the overall precision of the ladder alignment is on average 19 μm, whereas the distribution of the width of the unbiased residual distributions shows that the spatial resolution of the detector is improved by the alignment process down to $\sim 90\,\mu$m for the Top and Bottom boxes.

2.7.2 Number of Tracks

The second check performed is to compare the number of reconstructed tracks before and after alignment. In order to give a fair comparison, tight selection cuts are applied to both geometries:

- x search-window: 0.5 mm.
- y search-window: 7.0 mm.
- Maximum number of clusters per event: 5000.
- Track quality: $\chi^2/\text{dof} < 20$.

[6] In order to have a reliable fit on the distributions, higher statistics are needed. Therefore, the distributions of unbiased residuals separated by layer are used. The distributions per ladder were used for the study of the bias because the mean of the distribution is less sensitive to low statistics than its width.

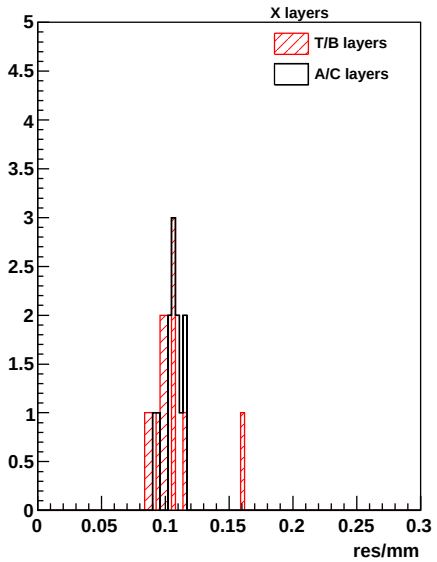

(a) X layers before alignment

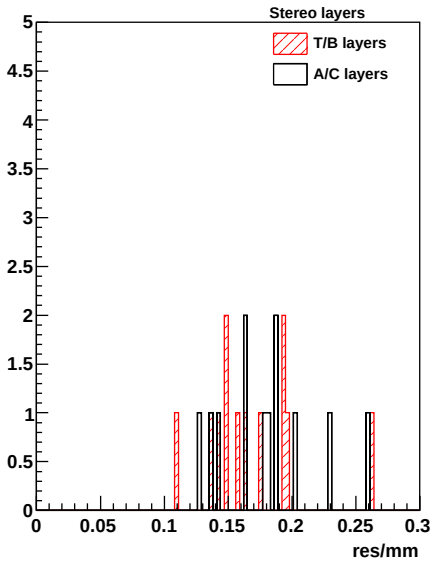

(b) stereo layers before alignment

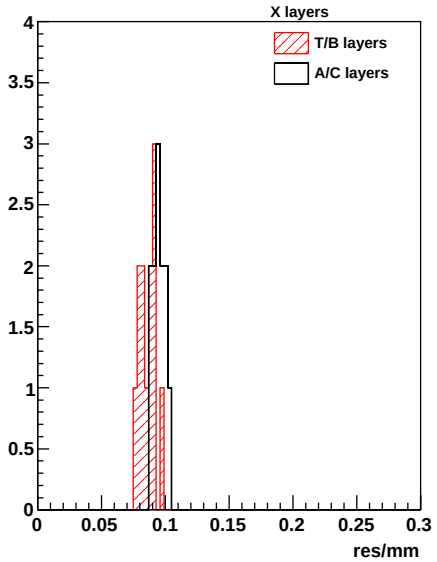

(c) X layers after alignment

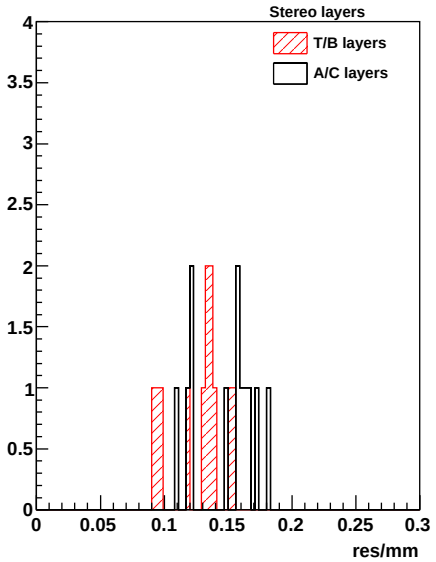

(d) stereo layers after alignment

Figure 24: Width of the distribution of unbiased residuals for individual layers: (a) X layers before alignment, (b) stereo layers before alignment, (c) X layers after alignment and (d) stereo layers after alignment.

Table 4: Number of tracks per box before and after the whole alignment procedure with TED data.

Geometry	A-side box	C-side box	Top box	Bottom box
Before alignment	2744	1339	697	559
After alignment	2927	1448	816	765
Gain	6.67 %	8.14 %	17.1 %	36.9 %

The data set used is the same as during the alignment procedure. The number of tracks per box before and after the whole alignment procedure can be seen in Table 4. The gain is higher for the Top and Bottom boxes, which indicates that the alignment of these boxes is more beneficial than for the side boxes. This can be related to the higher occupancy in the side boxes, as shown in Fig. 9, leading to a higher ghost rate and lower tracking efficiency. This, in turn, induces a worse alignment precision for the side boxes. Also, a higher occupancy means that the clone killing is more active in the side boxes than in the Top/Bottom boxes, reducing the gain due to the alignment. Finally, the larger increase for the Top/Bottom boxes is also due to the larger corrections determined for these boxes with respect to the A-/C-side boxes.

3 First Look at 2009 TED Data

New LHC synchronisation tests were performed in June 2009, giving the opportunity to validate the alignment parameters produced with the 2008 runs using an independent set of data. The main difference between the two runs is that the Inner Tracker is opened by $\sim 50\,\text{cm}$ in 2009 (see Fig. 25). In addition, most of the electronics-related faults shown in Fig. 21 were fixed (99 % channels are readout, compared to 97 % in 2008).

The first step is to add corrections to the 2008 aligned database in order to account for the shift of all the half-stations. To correct for any movements of the boxes during the opening or the maintenance of the detector, the boxes and layers were aligned using the histogram-based technique described in Ref. [3]. Corrections of $\sim 2\,\text{mm}$ for the boxes and $0.09\,\text{mm}$ for the layers were needed (compared to the $0.16\,\text{mm}$ for the layers discussed in Ref. [3] for the 2008 TED runs). After these the software procedure described in Section 2.1 is used.

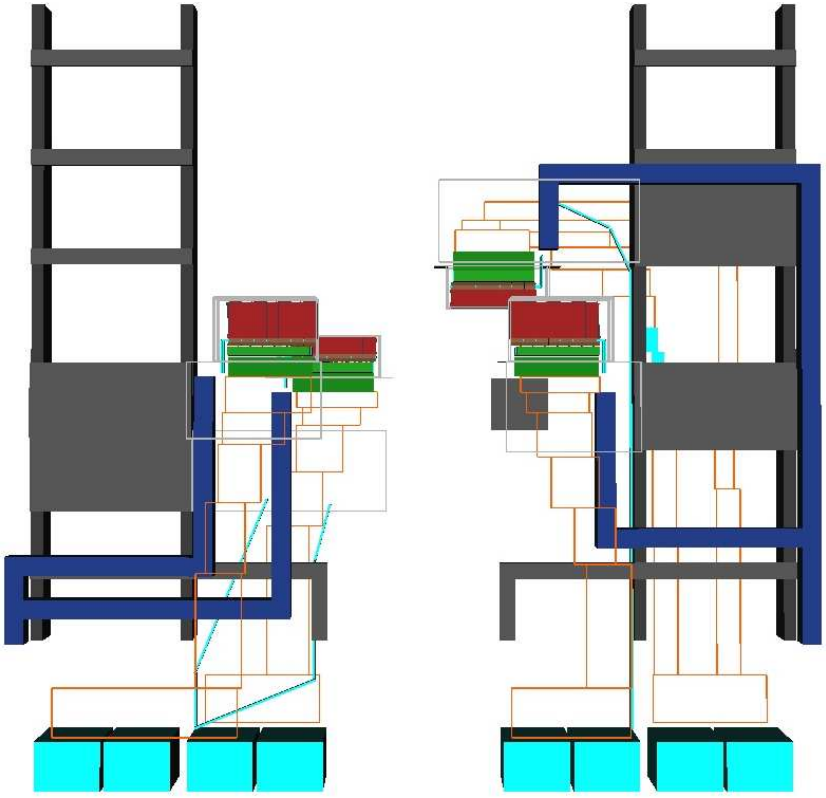

Figure 25: Layout of the Inner Tracker in the open position.

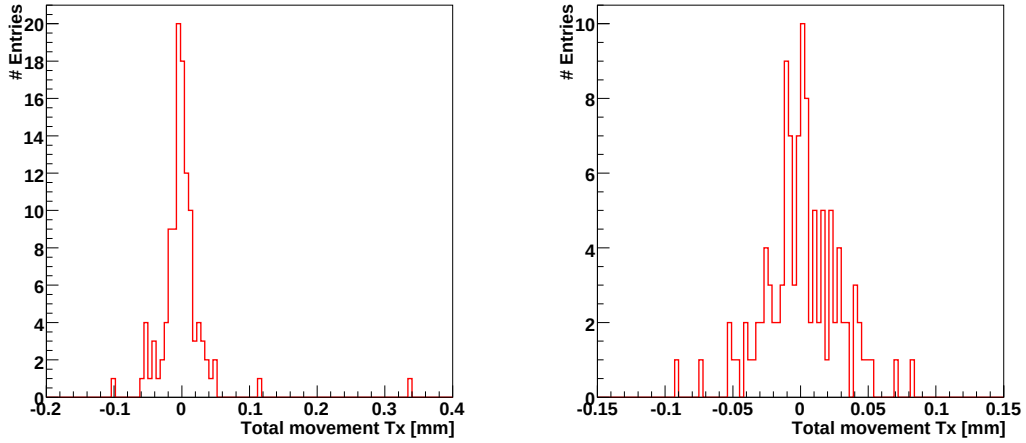

(a) A- and C-side ladder alignment (b) Top and Bottom ladder alignment

Figure 26: Distribution of the total movement in the alignment parameter Tx for all the ladders in the (a) A- and C-side boxes and (b) Top and Bottom boxes. Data from the 2009 TED runs are used.

The ladders are aligned using the software alignment process. The total movement after the eight iterations are shown in Fig. 26 for all ladders in (a) the A- and C-side boxes and (b) the Top and Bottom boxes. The RMS of these two distributions is 26 and 27 μm, respectively [7]. This agrees with the precision of the ladder Tx alignment of 19 μm quoted in Section 2.7.1.

4 Alignment with Cosmic Events

This section describes the studies performed on the alignment of the Inner Tracker using the cosmics data collected in August–September 2008.

4.1 Procedure

The alignment procedure with cosmics data, shown in Fig. 27, is similar to that for the TED data. The main difference is that the TrackCompetition

[7] The largest movement in plot (a), which corresponds to one of the two ladders that were repaired between the 2008 and the 2009 TED runs, is not taken into account.

algorithm after the track fit is not needed as the occupancy and hence ghost rate coming from wrong combinations is negligible. On the other hand, the tracking method creates clones that must be removed before the alignment algorithm is run. This clone killing is performed by the standard LHCb clone killing tool described in Ref. [9].

In this study, only the side boxes are aligned. No tracks are found in neither the Top and Bottom boxes because of the shorter strips and the angle of the cosmic rays. In order to remove the global unconstrained modes, the first two layers in Station 1 (X1 and U) and the last two layers in Station 3 (V and X2) are fixed to the value given by the first alignment given in Ref. [3]. However, the layers in Station 2 are also constrained by tracks going through Stations 1 and 2 on one hand and tracks going through Stations 2 and 3 on the other hand. The multi-step approach is not used here due to the lack of statistics.

4.2 Track and Event Selection

Due to the limited statistics of cosmic rays crossing at least two IT stations (and hence being reconstructible as tracks), the track selection cuts are kept loose (as described in Ref. [6]). A typical cosmic event is shown in Fig. 28. On the left-hand-side, a cosmic ray crossing the Outer Tracker, the Calorimeters and the Muon stations is shown. On the right-hand-side, the IT "golden track" crossing the three IT stations is represented in the $x - z$ plane.

In 2.6 millions events, only 82 tracks are found crossing at least two IT boxes in either the A- or the C-side sets of boxes. This is only ~ 40 tracks per stack, which gives a large statistical error and hence the results have poor precision. In this sample, only two tracks cross the three Inner Tracker boxes.

In order to reject the bad candidates that arise during the reconstruction process, two criteria are used. A confirmation from the calorimeters is required. If less than 300 MeV are deposited in the calorimeters by the track, it is discarded. Also, a loose χ^2 cut strategy is applied, starting from a cut at 250 and going down to 100. This way, bad tracks that pull some elements away are removed. Taking all these requirements into account, 64 tracks are used for the alignment of the two side boxes.

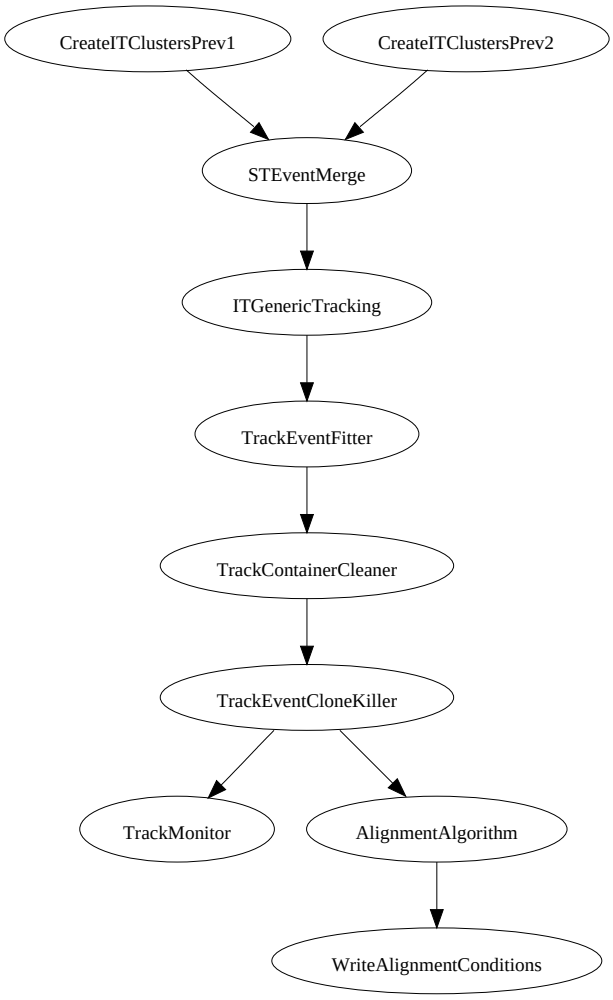

Figure 27: Flow diagram of the software procedure used for the tracking-station alignment with cosmics data.

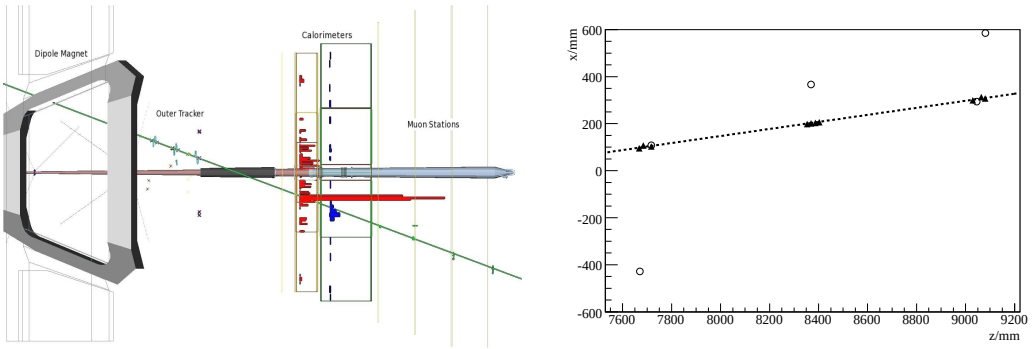

(a) (b)

Figure 28: Typical cosmics event display: (a) a cosmic ray crossing the Outer tracker, the Calorimeters and the Muon Stations and (b) the "golden cosmic ray" crossing the three IT stations.

4.3 Alignment Results

Figure 29 shows the evolution of the alignment parameters for the translation in x of the studied layers. Apart from two stereo layers in the C-side box of Station 2, the values of the alignment parameters are on average consistent with the initial values from the survey. However, oscillations coming from the limited statistics can be seen. This is clearly not satisfactory and shows the limitations of aligning the Inner Tracker with the current cosmics sample. For a meaningful alignment to be performed, a sample ten times larger would be necessary.

Two reasons can account for the huge movement of the two stereo layers in the C-side box. As explained in Section 4.1, the two first and two last layers are constrained. However, as described in Section 4.2, cosmics tracks only cross two boxes at a time. Due to the limited statistics, the constraint on the boxes in Station 2 from tracks crossing Stations 1 and 2 or Stations 2 and 3 is not sufficient to get rid of the weak mode. Tracks that interact in the detector material and have a kink in their trajectory could also explain such a behaviour. Cutting on the track fit quality will solve this problem. However, due to the low statistics, the cut had to be kept loose in order to keep enough tracks to align every layer with at least 10 hits.

This sample gives a proof of principle of the alignment method. Figures 30 (a) and (b) show respectively the distribution of unbiased residuals with respect to cosmic tracks before and after alignment. The number of selected tracks

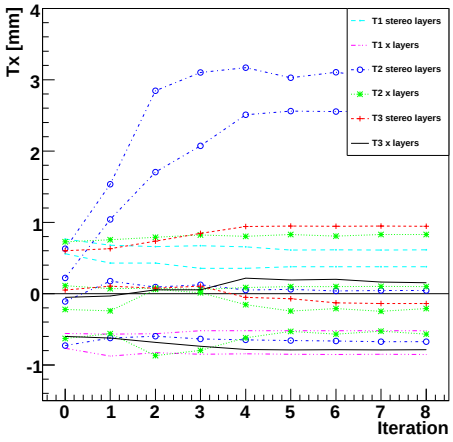

Figure 29: Evolution of the Tx alignment constants for all layers in A- and C-side stacks during layer alignment with cosmics data.

is lower with the aligned database than with the survey database. However, the unbiased residual distribution gets much narrower both for the A- and the C-Side boxes. Fitting a Gaussian through the histograms shows that the width of the distribution of unbiased residuals in the two boxes is reduced from 350 μm to 245 μm for the A-side box and from 230 μm to 185 μm for the C-side box.

5 Summary

The Inner Tracker has been aligned using the first tracks seen in the detector. These tracks were reconstructed using data taken during the LHC synchronisation tests of August–September 2008. Although the occupancy in the detector was high, a sample of good tracks was selected and used to internally align the Inner Tracker. At the ladder level, the alignment along the x direction is precise to 20 μm, compared to a single hit resolution of 57 μm. These results have been verified with the June 2009 TED run. Further studies on this data sample will be discussed in a subsequent note. Cosmics events collected over the same period have also been used but the statistics are too low to allow a precision alignment.

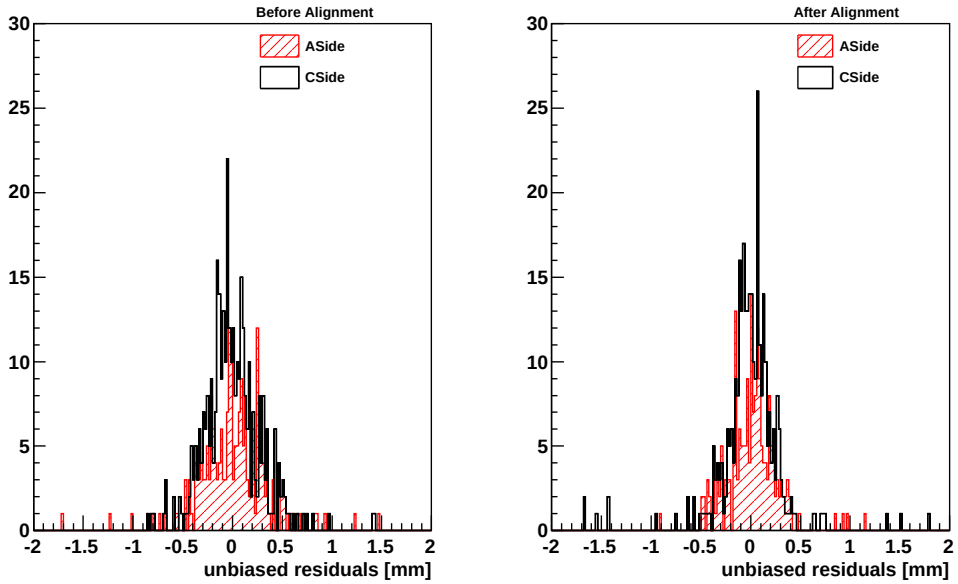

(a) before alignment (b) after alignment

Figure 30: Distribution of unbiased residuals for all hits on tracks. (a) shows the distribution with the surveyed geometry and (b) with the geometry obtained after layer alignment in Tx.

References

[1] LHCb Collaboration, *The LHCb Detector at LHC*, Journal of Instrumentation **3**, S08005 (2008).

[2] G. Conti and F. Blanc, *IT Survey Measurements Analysis and Implementation in the LHCb Software.*, CERN-LHCb-2008-069 (2008).

[3] M. Needham, *First Alignment of the Inner Tracker using Data from the TI-8 Sector Test*, CERN-LHCb-2009-030 (2009).

[4] L. Nicolas *et al.*, *First Studies of T-Station Alignment with Simulated Data*, CERN-LHCb-2008-065 (2009).

[5] J. Amoraal *et al.*, *Alignment Framework for LHCb based on Kalman-Filter Track-Fit Tracks*, LHCb note in preparation (2009).

[6] M. Needham, *Track Reconstruction in the LHCb Inner Tracker*, CERN-LHCb-PUB-2009-005 (2009).

[7] M. Merk *et al.*, *Performance of the LHCb OO Track Fitting*, LHCb-2000-086 (2000).

[8] M. Needham, *Classification of Ghost Tracks*, CERN-LHCb-2007-128 (2007).

[9] E. Rodrigues, *Dealing with Clones in the Tracking*, CERN-LHCb-2006-057 (2006).

[10] M.-O. Bettler *et al.*, *Assembly of the Inner Tracker Detector Boxes*, CERN-LHCb-2008-074 (2009).

A Unbiased Residuals Distributions per Layer during the Alignment with TED Data

The distributions of unbiased residuals in the IT layers obtained with Inner Tracker tracks from the TED data have been fitted individually with a Gaussian. Figure 31 shows the distribution of the bias of these Gaussian fits. The X and stereo layers are shown separately. The fit has been performed on the distribution both before and after alignment. A clear improvement is visible after the alignment procedure, as was already visible with the distributions separated by ladders, shown in Section 2.7.1.

B TT Confirmation of the IT Alignment Results with TED Data

Another method investigated to validate the results of the Inner Tracker alignment is to propagate the tracks found in the Inner Tracker to the Tracker Turicensis (TT) [1]. The distribution of the residuals of TT hits with respect to the extrapolated IT tracks should indeed improve during the alignment process. The resolution of the distribution is then reported at each step of the alignment (before alignment, after box, layer and ladder alignment). This has been performed using an independent data sample which included hits in the TT.

Figure 32 shows the evolution of (a) the residuals in the layer TTaX with respect to tracks going through the IT Top box, and (b) the residuals in the layer TTbV with respect to tracks going through the IT A-side box.

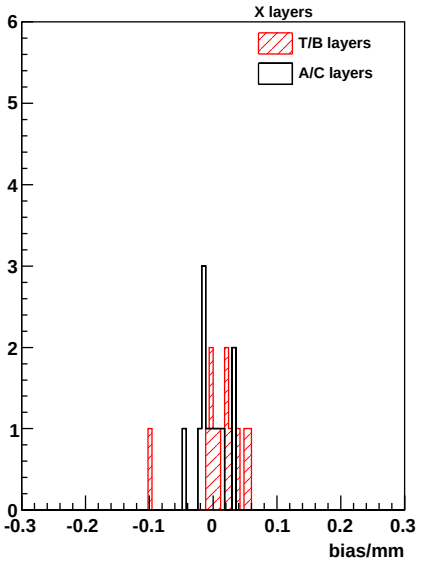

(a) X layers before alignment

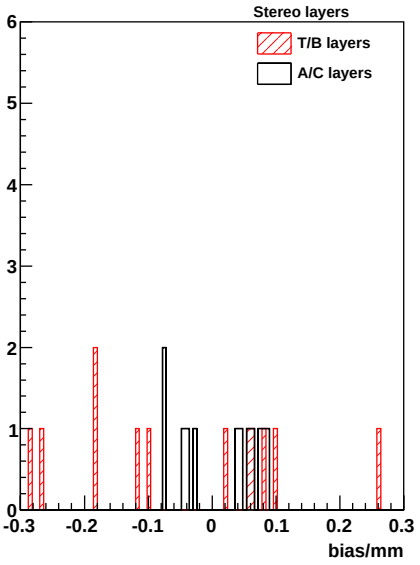

(b) stereo layers before alignment

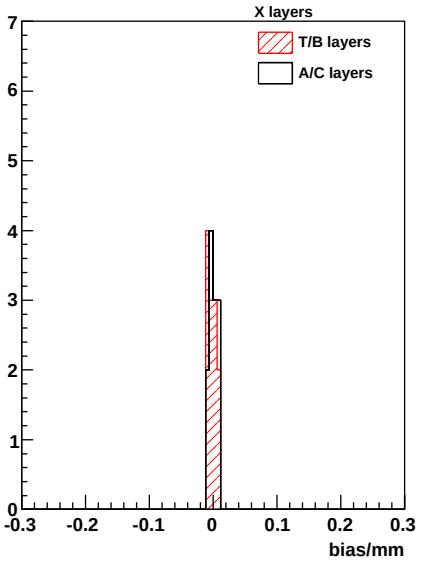

(c) X layers after alignment

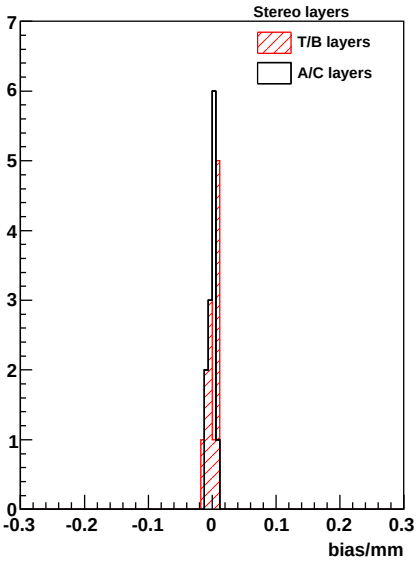

(d) stereo layers after alignment

Figure 31: Bias of the distribution of unbiased residuals for individual IT layers. (a) shows the X layers before alignment, (b) the stereo layers before alignment, (c) the X layers after alignment and (d) the stereo layers after alignment.

Although the first plot shows a nice evolution, with the resolution decreasing at each alignment step, it has to be noted that most of the other evolution plots look more like the second plot.

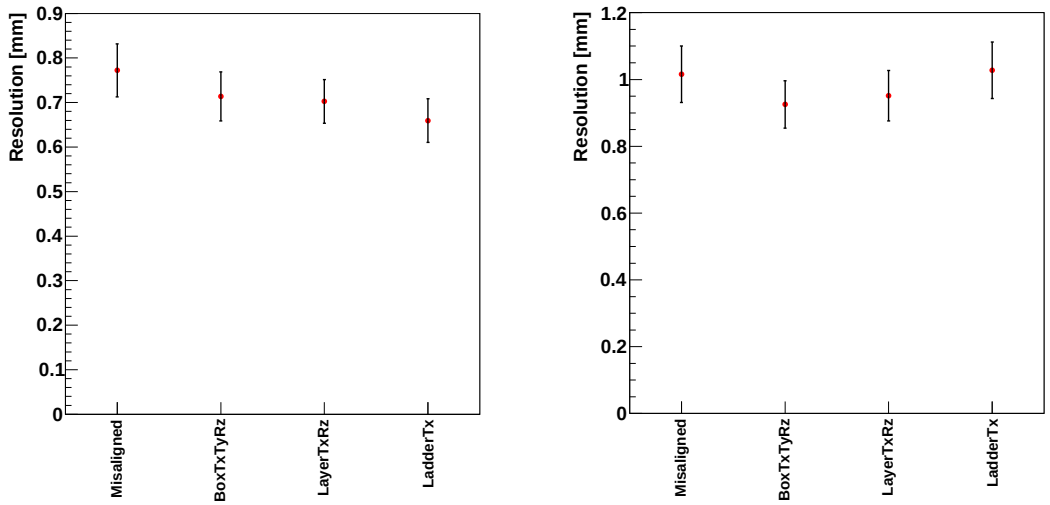

(a) TTaX hits vs IT Top tracks (b) TTbV hits vs IT A-side tracks

Figure 32: Evolution of the resolution of the distributions of residuals of TT hits with respect to tracks going through IT. The plot on the left shows the residuals in the TTaX layer with respect to tracks from IT Top box. The plot on the right shows the residuals in the TTbV layer with respect to tracks coming from the IT A-side box.

The fact that most of the evolution plots do not behave as expected (the resolution should improve at each alignment step) shows that the confirmation using TT information is not as powerful as the unbiased residuals. This is due to several reasons. During the whole alignment process, several layers are fixed. This means that the alignment is only internal to the Inner Tracker but doesn't account for any global movement (whether it be a translation, a rotation, a shearing or a more complex movement) of the Inner Tracker boxes, layers or modules. This means, in particular, that the Inner Tracker is not aligned with respect to the rest of the LHCb detector (for example the TT used here).

Another reason for the worse performance of the TT confirmation is that this sub-detector has not been internally aligned prior to this study. This effect should be smaller than the first one as alignment corrections to the survey measurements are expected to be small for the TT.

Finally, due to the large propagation distance between the Inner Tracker and the Tracker Turicensis, a rotation of the former during alignment induces a worse resolution in the latter. This problem will be solved when relative TT–IT alignment will be performed.